former part of extinction training; 3) intra-BLA infusions of *Arc* antisense ODN before extinction training impaired long-term but not short-term extinction memory; and 4) intra-BLA infusions of *Arc* antisense ODN 3 h after extinction training had no effect on fear extinction. Collectively, these findings indicate that de novo Arc expression, induced by extinction training, contributes to long-term extinction of contextual conditioned fear.

Our study design suggests that this impaired extinction of conditioned fear cannot be explained by a nonspecific effect of intra-BLA infusions of *Arc* antisense ODN. First, the Arc antisense ODN effectively inhibited Arc expression and exhibited a high degree of specificity for *Arc* relative to other immediate-early genes (IEGs) (Additional file 1). Second, the behavior of the mice that received *Arc* antisense ODN during extinction training and the short-term memory test was comparable to that of the mice that received scrambled ODN, indicating that the antisense ODN had no effect on retrieval of fear memory and acquisition of extinction memory. More importantly, fear extinction in the mice that received *Arc* antisense ODN 3 h after extinction training was intact, indicating that extinction training-induced *Arc* translation is essential for fear extinction.

Arc may contribute to fear extinction by reducing synaptic strength. Fear memory is thought to be maintained by fear conditioning-induced potentiation of synaptic efficacy in amygdalar synapses [15,16]. Extinction training reverses this potentiation through accelerated endocytosis of AMPAR [5]. This endocytosis-regulated depotentiation is likely an essential mechanism for fear extinction, because inhibiting AMPAR endocytosis impairs fear extinction [5,6]. In this study, we found that Arc expression is required for fear extinction. Arc interacts with endophilin and dynamin to modulate AMPAR endocytosis [11], thus allowing Arc to influence synaptic strength and homeostasis [9,17]. Taken as a whole, extinction training induces Arc expression, which possibly accelerates AMPAR endocytosis and reverses fear conditioning-induced synaptic potentiation. The resulting depotentiation is likely to contribute to fear extinction.

In short, our findings provide evidence that Arc is critical for long-term extinction of conditioned fear, and that activation of Arc signaling in the BLA might lead to long-term extinction of fear memory through reversal of fear conditioning-induced synaptic potentiation. A better understanding of the mechanisms underlying fear extinction is necessary for the development of new treatments for psychiatric disorders such as post-traumatic stress disorder. These data suggest that a BLA Arc-regulated pathway could generate viable targets for these potential new therapies.

Materials and methods

Animal experiment ethics

All experiments were approved by the animal experiment ethics committee at the University of Tokyo (approval number 24–10), and were in accordance with the University of Tokyo guidelines for the care and use of laboratory animals.

Subjects

Male C57BL/6J mice (Japan SLC Inc., Shizuoka, Japan), weighing 20–30 g and aged 8–13 weeks, were housed 2–4 per cage, and kept on a 12-h light/dark cycle (lights on from 7:00 a.m. to 7:00 p.m.). They were given free access to food and water, and acclimated to daily handling for 1 week prior to the start of the study.

Behavioral procedure

Contextual fear conditioning, extinction training, and subsequent testing were performed in a conditioning chamber (17 cm wide, 15 cm deep, and 15 cm high) with a stainless steel grid floor (O' Hara & Co., Ltd, Tokyo, Japan). A conditioning session consisted of placing the animal in the chamber and delivering a 2-s foot shock (0.3 mA) after 130 s. The mice then received 2 additional shocks every 100 s. They were kept in the chamber for an additional 50 s and were then returned to their home cage. For extinction training and testing, mice were re-exposed to the conditioning chamber without shock. All sessions were performed between 9:00 a.m. and 1:00 p.m., and each session was video-recorded for automatic scoring of freezing as described previously [18].

In Experiment 1, mice in the Extinction group underwent 40 min of extinction training 24 h after fear conditioning and were killed 90 min later. Mice in the No Extinction group received fear conditioning, and 1 day later, they were killed immediately following removal from the home cage. Their brain slices were subjected to Arc immunohistochemistry.

In Experiment 2, mice in the Extinction group underwent 35 min of extinction training 24 h after fear conditioning and were killed immediately after extinction training. Their brain slices were subjected to *Arc* fluorescent *in situ* hybridization.

In Experiment 3, we examined the effect and specificity of *Arc* antisense ODN. Mice received *Arc* antisense or scrambled ODN infusions into the hippocampus and underwent fear conditioning 1.5 or 3 h later. Mice were decapitated after diethyl ether anesthesia 2 h after fear conditioning, and their brains were rapidly removed and frozen at −80°C. Coronal brain sections (300 μm) were prepared using a cryostat. The dorsal hippocampus (1.30 to 1.90 mm posterior to bregma) was punched out and homogenized in RIPA buffer (08714–04, Nacalai Tesque, Kyoto, Japan).

In Experiment 4, mice underwent extinction training 24 h after fear conditioning. To determine if Arc inhibition affected fear extinction, mice received intra-BLA infusions of either *Arc* antisense or scrambled ODN 3 h before extinction training, and were subjected to a short-term and long-term memory tests 2 h and 24 h later, respectively.

In Experiment 5, mice underwent extinction training 24 h after fear conditioning. To assess the effect of the post-extinction training time interval, mice received intra-BLA infusions of either *Arc* antisense or scrambled ODN 3 h after extinction training and were subjected to a long-term memory test 24 h later.

Microinfusions

Surgery for intra-BLA infusions was conducted according to our previous study [19]. Briefly, mice were anesthetized with pentobarbital (2.5 mg/kg, i.p.) and xylazine (10 mg/kg, i.p.), and 26-gauge stainless-steel guide cannulae (Plastics One, VA, USA) were implanted in the BLA (AP = −1.4, ML = ±3.5, DV = −4.8 mm relative to bregma). Mice were given at least 7 days of postoperative recovery time. Microinfusions of *Arc* antisense or scrambled ODN (400 pmol; 0.5 μL/side) were made over 2 min, and the infusion cannulae were left in place for at least 2 min afterwards in order to facilitate the diffusion of ODN throughout the whole BLA.

Arc antisense ODN and scrambled ODN (GeneDesign Inc, Osaka, Japan) were designed in reference to a previous study [14]. The *Arc* ODN encoded an antisense sequence for the *Arc* mRNA sequence near the translation start site [7]. The scrambled ODN does not show significant homology to any sequences in the GenBank database [14]. Both ODNs contained phosphorothioate linkages on the three terminal bases of both the 5′ and 3′ ends, and phosphodiester internal bonds. This design is reported more stable than unmodified phosphorothioated ODNs in vivo, and less toxic than fully phosphorothioated ODNs [14]. The following sequences were used ("~" denotes a phosphorothioate linkage): 5′-G~T~C~CAGCTC CATCTGGT~C~G~T-3′ (antisense) and 5′-C~G~T~G CACCTCTCGCAGG~T~T~T-3′ (scrambled).

In the Experiment 3, the guide cannulae were implanted in the dorsal hippocampus (−2.0, ±1.7, −2.1 mm relative to bregma).

Immunohistochemistry and image analysis

After the anesthetization, mice were transcardially perfused with PBS followed by 4% paraformaldehyde (PFA). Brains were post-fixed in 4% PFA for 12 h. Free-floating coronal sections (40 μm) were prepared using a cryostat (HM520; Thermo Fisher Scientific, Waltham, MA, USA). Arc was visualized with anti-Arc primary antibody (1:1,000; SySy, Gottingen, Germany), biotinylated anti-rabbit secondary antibody (1:500; Vector Laboratories, Burlingame, CA, USA), VECTASTAIN ABC Kit (Vector Laboratories), and Cy3-tyramide (1:100; Perkin-Elmer, Waltham, MA, USA). Nuclei were counterstained with Hoechst dye (1:1000; Invitrogen).

Images of the amygdala were acquired by z-stacks using a confocal microscope (CV1000; YOKOGAWA, Tokyo, Japan) at 40 × under an oil-immersion lens (NA 1.3). Images of BA and LA from three sections (1.34, 1.58, 1.82 mm posterior to bregma) per mouse were analyzed using ImageJ (NIH).

Fluorescent *in situ* hybridization and image analysis

After the mice were sacrificed, the brains were frozen quickly and stored at −80°C until further processing. Brains were sectioned (20 μm) with a cryostat, mounted on slides and stored at −80°C. Antisense riboprobes for *Arc*, conjugated to digoxigenin-UTP (Roche Applied Science, Penzberg, Germany), were generated from cDNA plasmid (provided by Dr. Paul F Worley) containing an almost full-length cDNA of the *Arc* transcript using MAXIScript (Ambion, Austin, TX USA). *In situ* hybridization was performed according to previously published protocols [20]. Slide-mounted brain sections were fixed in 4% PFA, acetylated with 0.5% acetic anhydride/1.5% triethanolamine, dehydrated through 50% methanol/50% acetone solutions, and equilibrated in 2× saline sodium citrate buffer (SSC). Slides were incubated in prehybridization buffer for 30 min. The antisense riboprobe was diluted to 150 μL in hybridization buffer, heat denatured, chilled on ice, and applied to each slide. Hybridization was carried out at 56°C for 16 h. Slides were washed to a final stringency of 0.5×SSC at 56°C, which included an earlier wash step at 37°C in 2×SSC with RNase A (10 μg/mL). Endogenous peroxidase activity was quenched with 2% H_2O_2 in 1×SSC. Slides were blocked with TSA blocking reagent (PerkinElmer, Waltham, MA, USA) and incubated with an anti-digoxigenin horseradish peroxidase conjugate (1:500, Roche) for 2 h. Slides were washed three times in Tris-buffered saline with 0.05% Tween-20, and incubated with fluorescein-tyramine working solution (1:10, PerkinElmer). Slides were washed in PBS and the nuclei were counterstained with propidium iodide (PI, 10 μM; Life Technologies) for 10 min. Finally, the sections were washed with PBS and mounted in Permafluor (Thermo Fisher Scientific, Waltham, MA, USA).

Images of the BLA (1.58 mm posterior to bregma) were acquired by collecting z-stacks using a confocal microscope (LSM-510; Zeiss, Oberkochen, Germanay) at 40× under an water-immersion lens (NA 1.2) and analyzed using in-house Matlab program. From 4 to 8 sections per mouse were counted for the analysis. Only cells that contained whole nuclei and were presumptive neurons, with large nuclei stained diffusely with propidium

iodide, were included in the analysis. The designation "nuclear *Arc* positive" was assigned to neurons that exhibited 1 or 2 of the characteristic intense intranuclear areas of fluorescence; the designation "cytoplasmic *Arc* positive" was assigned to neurons that contained perinuclear/cytoplasmic labeling over multiple optical sections. Labels were assigned by an experimenter blind to behavioral conditions.

Western blotting

Protein concentrations were normalized across homogenates using a Bradford assay. Equal amounts of protein were electrophoresed on 5-20% SDS polyacrylamide gels and transferred to PVDF membranes. Western blots were blocked in blocking buffer (03953–95, Nacalai Tesque) and then incubated with an anti-*beta*-actin antibody (1:1000; A5441, Sigma), an anti-Arc/Arg3.1 antibody (1:1000; sc-17839, Santa Cruz Biotechnology), anti-c-Fos antibody (1:100; Ab-2, Calbiochem) or anti-Zif268 antibody (1:1000; #4153, Cell Signaling). After incubation with anti-mouse IgG (1:100000; A9044, Sigma) or anti-rabbit IgG (1:10000; 01827–44, Nacalai Tesque), bands were developed with a chemiluminescent substrate (RPN2132, GE Healthcare). The immunopositive signals were detected by ImageQuant LAS 4000 (GE Healthcare) and analyzed using ImageJ (NIH).

Data analysis

All values were reported as mean ± SEM. Statistical analysis was performed using Student's *t*-test, repeated-measures ANOVA, one-way ANOVA and Tukey's test.

Additional file

Additional file 1: *Arc* antisense ODN infusions inhibit Arc expression but not c-Fos or Zif268 expression. Mice were infused with Arc antisense or scrambled ODN 1.5 h or 3 h before conditioning. Mice were killed 2 h after conditioning. Control mice received fear conditioning without infusions. Arc, c-Fos and Zif268 levels were normalized with the level of control mice. **(A)** *Arc* antisense ODN infusions 3 h but not 1.5 h before conditioning decreased Arc levels (One-way ANOVA, $F_{(2,15)} = 10.8$, $p = 0.0012$; post-hoc Tukey's test, Scrambled vs. Antisense (3 h), $p = 0.0017$). **(B, C)** These infusions did not affect c-Fos or Zif268 levels (c-Fos, $t_{(10)} = 0.91$, $p = 0.38$; Zif268, $t_{(10)} = 0.85$, $p = 0.41$). $^{**}p < 0.01$.

Abbreviations

Arc: Activity-regulated cytoskeletal-associated protein; CREB: cAMP response element binding protein; AMPAR: α-amino-3-hydroxy-5-methyl-4-isoxazolepropionic acid receptor; BLA: Basolateral amygdala; BA: Basal amygdala; LA: Lateral amygdala; STM: Short-term memory; LTM: Long-term memory; ODN: Oligodeoxynucleotide; IEGs: Immediate-early genes; PFA: Paraformaldehyde; catFISH: cellular analysis of temporal activity by fluorescence *in situ* hybridization.

Competing interests

The authors declare that they have no competing interests.

Authors' contributions

KO, DN and HN performed experiments and analyzed the data. DN and HN designed the study. KO and HN wrote the manuscript. NM and YI supervised the project. All authors read and approved the final manuscript.

Acknowledgements

We thank Dr. Paul F Worley for the *Arc* cDNA. This work was supported by Grant-in-Aid for Young Scientists (B) (25830002, to HN), Grant-in-Aid for Scientific Research on Innovative Areas, "Mesoscopic Neurocircuitry" (No. 23115101, to HN), "The Science of Mental Time" (No. 26119507 to HN and No. 25119004 to YI) and "Memory Dynamism" (No. 26115509 to HN).

Author details

[1]Laboratory of Chemical Pharmacology, Graduate School of Pharmaceutical Sciences, The University of Tokyo, 7-3-1 Hongo, Bunkyo-ku, Tokyo 113-0033, Japan. [2]Center for Information and Neural Networks, Suita, Osaka 565-0871, Japan.

Received: 24 December 2013 Accepted: 16 April 2014
Published: 23 April 2014

References

1. Mamiya N, Fukushima H, Suzuki A, Matsuyama Z, Homma S, Frankland PW, Kida S: **Brain region-specific gene expression activation required for reconsolidation and extinction of contextual fear memory.** *J Neurosci* 2009, **29**(2):402–413.
2. Vianna MR, Szapiro G, McGaugh JL, Medina JH, Izquierdo I: **Retrieval of memory for fear-motivated training initiates extinction requiring protein synthesis in the rat hippocampus.** *Proc Natl Acad Sci U S A* 2001, **98**(21):12251–12254.
3. Orsini CA, Maren S: **Neural and cellular mechanisms of fear and extinction memory formation.** *Neurosci Biobehav Rev* 2012, **36**(7):1773–1802.
4. Quirk GJ, Repa C, LeDoux JE: **Fear conditioning enhances short-latency auditory responses of lateral amygdala neurons: parallel recordings in the freely behaving rat.** *Neuron* 1995, **15**(5):1029–1039.
5. Kim J, Lee S, Park K, Hong I, Song B, Son G, Park H, Kim WR, Park E, Choe HK, Kim H, Lee C, Sun W, Kim K, Shin KS, Choi S: **Amygdala depotentiation and fear extinction.** *Proc Natl Acad Sci U S A* 2007, **104**(52):20955–20960.
6. Dalton GL, Wang YT, Floresco SB, Phillips AG: **Disruption of AMPA receptor endocytosis impairs the extinction, but not acquisition of learned fear.** *Neuropsychopharmacology* 2008, **33**(10):2416–2426.
7. Lyford GL, Yamagata K, Kaufmann WE, Barnes CA, Sanders LK, Copeland NG, Gilbert DJ, Jenkins NA, Lanahan AA, Worley PF: **Arc, a growth factor and activity-regulated gene, encodes a novel cytoskeleton-associated protein that is enriched in neuronal dendrites.** *Neuron* 1995, **14**(2):433–445.
8. Link W, Konietzko U, Kauselmann G, Krug M, Schwanke B, Frey U, Kuhl D: **Somatodendritic expression of an immediate early gene is regulated by synaptic activity.** *Proc Natl Acad Sci U.S.A* 1995, **92**(12):5734–5738.
9. Shepherd JD, Bear MF: **New views of Arc, a master regulator of synaptic plasticity.** *Nat Neurosci* 2011, **14**(3):279–284.
10. Rial Verde EM, Lee-Osbourne J, Worley PF, Malinow R, Cline HT: **Increased expression of the immediate-early gene arc/arg3.1 reduces AMPA receptor-mediated synaptic transmission.** *Neuron* 2006, **52**(3):461–474.
11. Chowdhury S, Shepherd JD, Okuno H, Lyford G, Petralia RS, Plath N, Kuhl D, Huganir RL, Worley PF: **Arc/Arg3.1 interacts with the endocytic machinery to regulate AMPA receptor trafficking.** *Neuron* 2006, **52**(3):445–459.
12. Kawashima T, Okuno H, Nonaka M, Adachi-Morishima A, Kyo N, Okamura M, Takemoto-Kimura S, Worley PF, Bito H: **Synaptic activity-responsive element in the Arc/Arg3.1 promoter essential for synapse-to-nucleus signaling in activated neurons.** *Proc Natl Acad Sci U.S.A* 2009, **106**(1):316–321.
13. Maddox SA, Schafe GE: **The activity-regulated cytoskeletal-associated protein (Arc/Arg3.1) is required for reconsolidation of a Pavlovian fear memory.** *J Neurosci* 2011, **31**(19):7073–7082.
14. Guzowski JF, Lyford GL, Stevenson GD, Houston FP, McGaugh JL, Worley PF, Barnes CA: **Inhibition of activity-dependent arc protein expression in the rat hippocampus impairs the maintenance of long-term potentiation and the consolidation of long-term memory.** *J Neurosci* 2000, **20**(11):3993–4001.
15. McKernan MG, Shinnick-Gallagher P: **Fear conditioning induces a lasting potentiation of synaptic currents in vitro.** *Nature* 1997, **390**(6660):607–611.
16. Rogan MT, Staubli UV, LeDoux JE: **Fear conditioning induces associative long-term potentiation in the amygdala.** *Nature* 1997, **390**(6660):604–607.
17. Shepherd JD, Rumbaugh G, Wu J, Chowdhury S, Plath N, Kuhl D, Huganir RL, Worley PF: **Arc/Arg3.1 mediates homeostatic synaptic scaling of AMPA receptors.** *Neuron* 2006, **52**(3):475–484.

18. Nomura H, Matsuki N: **Ethanol enhances reactivated fear memories.** *Neuropsychopharmacology* 2008, **33**(12):2912–2921.
19. Nakayama D, Yamasaki Y, Matsuki N, Nomura H: **Post-retrieval late process contributes to persistence of reactivated fear memory.** *Learn Mem* 2013, **20**(6):307–310.
20. Nomura H, Nonaka A, Imamura N, Hashikawa K, Matsuki N: **Memory coding in plastic neuronal subpopulations within the amygdala.** *Neuroimage* 2012, **60**(1):153–161.

doi:10.1186/1756-6606-7-30
Cite this article as: Onoue *et al.*: Fear extinction requires Arc/Arg3.1 expression in the basolateral amygdala. *Molecular Brain* 2014 **7**:30.

J Physiol 592.13 (2014) pp 2771–2783

JPn Neuroscience The Journal of Physiology

Astrocyte calcium signalling orchestrates neuronal synchronization in organotypic hippocampal slices

Takuya Sasaki[1], Tomoe Ishikawa[1], Reimi Abe[1], Ryota Nakayama[1], Akiko Asada[1], Norio Matsuki[1] and Yuji Ikegaya[1,2]

[1]*Graduate School of Pharmaceutical Sciences, University of Tokyo, Tokyo, Japan*
[2]*Center for Information and Neural Networks, Suita City, Osaka, Japan*

Key points

- In the brain, astrocytes detect neuronal activity and regulate neuronal excitability and synaptic transmission.
- Recent studies show that calcium elevations that are localized within astrocyte processes upregulate endogenous neurotransmission at nearby synapses.
- We demonstrated that at the network level calcium buffering in astrocytes caused a significant reduction in the correlated activity of neurons in cultured hippocampal slices.
- In contrast, the uncaging of calcium in astrocytes triggered synchronized activity in neuronal populations.
- This study provides experimental support for the functional relevance of astrocyte signalling to the maintenance of collective neuronal dynamics.

Abstract Astrocytes are thought to detect neuronal activity in the form of intracellular calcium elevations; thereby, astrocytes can regulate neuronal excitability and synaptic transmission. Little is known, however, about how the astrocyte calcium signal regulates the activity of neuronal populations. In this study, we addressed this issue using functional multineuron calcium imaging in hippocampal slice cultures. Under normal conditions, CA3 neuronal networks exhibited temporally correlated activity patterns, occasionally generating large synchronization among a subset of cells. The synchronized neuronal activity was correlated with astrocyte calcium events. Calcium buffering by an intracellular injection of a calcium chelator into multiple astrocytes reduced the synaptic strength of unitary transmission between pairs of surrounding pyramidal cells and caused desynchronization of the neuronal networks. Uncaging the calcium in the astrocytes increased the frequency of neuronal synchronization. These data suggest an essential role of the astrocyte calcium signal in the maintenance of basal neuronal function at the circuit level.

(Received 12 February 2014; accepted after revision 6 April 2014; first published online 7 April 2014)
Corresponding author T. Sasaki: Laboratory of Chemical Pharmacology, Graduate School of Pharmaceutical Sciences, University of Tokyo, Hongo 7-3-1, Bunkyo-ku, Tokyo, Japan. E-mail: t.sasaki.0224@gmail.com.

Abbreviations aCSF, artificial cerebrospinal fluid; AP5, (2*R*)-amino-5-phosphonopentanoate; GFAP, glial fibrillary acidic protein; IEI, inter-event interval; MCPG, (*S*)-α-methyl-4-carboxyphenylglycine; mGluR, metabotropic glutamate receptor; NMDA, *N*-methyl-D-aspartate; NP-EGTA, *o*-nitrophenyl-EGTA; PFA, paraformaldehyde; PPADS, pyridoxal-phosphate-6-azophenyl-2′,4′-disulphonic acid.

Introduction

Brain function occurs through the concerted activity of neuronal and glial circuitry (Allen & Barres, 2009). Whereas neurons use electrical signals across the plasma membrane, astrocytes, the largest class of glial cells, exhibit excitability in the form of changes in intracellular calcium concentrations. Astrocyte calcium transients can be induced by synaptic activity *in vitro* (Perea & Araque, 2005; Gordon *et al.* 2009; Bernardinelli *et al.* 2011; Min

DOI: 10.1113/jphysiol.2014.272864

& Nevian, 2012) and sensory-evoked stimulation *in vivo* (Wang *et al.* 2006; Schummers *et al.* 2008; Nimmerjahn *et al.* 2009; Takata *et al.* 2011). Astrocyte calcium transients modulate synaptic transmission and plasticity through the extracellular release of gliotransmitters (Halassa & Haydon, 2010; Henneberger *et al.* 2010).

In addition to the previously accumulated evidence, recent studies have shown that calcium elevations that occur within astrocyte processes can be triggered by the basal synaptic activity associated with single action potentials. These localized calcium signals are believed to upregulate the endogenous neurotransmission at nearby synapses (Di Castro *et al.* 2011; Panatier *et al.* 2011). Single astrocytes contact thousands of synapses; thus, astrocytes may work as a key component that sustains neuronal circuit function. However, little was known about the impact of astrocyte calcium signalling on the collective dynamics of a large number of neurons. To address this issue, it is necessary to capture the many-to-many relationship between neuronal and astrocytic populations.

In this study, we used functional multineuron calcium imaging and intracellular dialysis of a calcium chelator and examined how disrupting the astrocyte calcium signal affected the spatiotemporal activity patterns of neuron populations in cultured hippocampal slices. Inhibiting the astrocyte calcium signalling significantly suppressed neuronal network synchronization, which was measured by two parameters: the frequency of large synchronization events and the number of correlated neuron pairs.

Methods

Ethical approval

Experiments were performed with the approval of the animal experimental ethics committee at the University of Tokyo (approval number: 24-6) according to the University of Tokyo guidelines for the care and use of laboratory animals.

Slice preparations

Hippocampal slice cultures were prepared from postnatal day 7 Wistar/ST rats ($n = 32$) (SLC, Shizuoka, Japan). Briefly, rat pups were chilled, and the brains were removed and horizontally cut into 300 μm-thick slices in aerated, ice-cold Gey's balanced salt solution supplemented with 25 mM glucose. Entorhino-hippocampal stumps were excised and cultivated on Omnipore membrane filters (JHWP02500; Millipore, Billerica, MA, USA) that were laid on plastic O-ring discs (Koyama *et al.* 2007). The cultures were fed with 1 ml of 50% minimal essential medium, 25% Hanks' balanced salt solution, 25% horse serum and antibiotics in a humidified incubator at 37°C in 5% CO_2 and were used for experiments on days 7–14 *in vitro*. The medium was changed every 3.5 days.

Calcium imaging from cultured slices

Slices were washed three times with oxygenated artificial cerebrospinal fluid (aCSF) consisting of (mM) 127 NaCl, 26 $NaHCO_3$, 3.3 KCl, 1.24 KH_2PO_4, 1.2 $MgSO_4$, 1.2–1.5 $CaCl_2$ and 10 glucose, and bubbled with 95% O_2 and 5% CO_2, unless otherwise specified. The slices were transferred to a 35 mm dish filled with 2 ml of dye solution and incubated for 40 min in a humidified incubator at 37°C in 5% CO_2 with 0.0005% Oregon Green 488 BAPTA-1 (OGB-1) AM (Invitrogen, Carlsbad, CA, USA), 0.01% Pluronic F-127 (Invitrogen) and 0.005% Cremophor EL (Sigma-Aldrich, St Louis, MO, USA). The slices were then covered in aCSF again for >30 min. The slices were mounted in a recording chamber at 32°C and perfused with aCSF at a rate of 1.5–2.0 ml min^{-1} for >15 min. The hippocampal CA3 pyramidal cell layer was imaged at 10 Hz using a Nipkow-disc confocal microscope (CSU-X1; Yokogawa Electric, Tokyo, Japan), a cooled CCD camera (iXonEM$^+$ DV897; Andor Technology, Belfast, UK), an upright microscope with a water-immersion objective lens (16×, 0.8 numerical aperture; Nikon). The fluorophores were excited at 488 nm with a laser diode and visualized with a 507 nm long-pass emission filter. After identification of the cell types, the regions of interest were carefully placed onto the cell bodies. The fluorescence change ($\Delta F/F$) was calculated as $\Delta F/F = (F_t - F_0)/F_0$, where F_t is the fluorescence intensity at time t, and F_0 is the baseline intensity averaged for 50 s before and after time t. Spike times were reconstructed from the onsets of Ca^{2+} transients with custom-written software in Microsoft Visual Basic (Sasaki *et al.* 2008). The signals were then inspected by eye to remove erroneously detected noise. For astrocytes, the region of interest size was set to a diameter of 10 μm, which corresponds to the size of the astrocyte soma. Calcium elevations were extracted with a threshold of 4 × SD of the baseline noise and a 5 s duration (Sasaki *et al.* 2011). The signals were then inspected by eye to remove erroneously detected noise. Data analysis was performed with custom software written in Matlab (Mathworks, Natick, MA, USA). (*S*)-α-Methyl-4-carboxyphenylglycine (MCPG; Sigma-Aldrich), pyridoxal-phosphate-6-azophenyl-2′,4′-disulphonic acid (PPADS; Sigma-Aldrich) and (2*R*)-amino-5-phosphonopentanoate (AP5) were applied in the bath.

In vivo calcium imaging of rat hippocampal astrocytes

Male Wistar rats (postnatal, 14 days old; $n = 6$) were anaesthetized with urethane (1.5 g kg^{-1}, I.P.), and the exposed skull was glued to a metal plate, which was fixed to

a stereotaxic frame. A craniotomy (2.5 to 3 mm diameter), centred 3.0 mm posteriorly and 2.5 mm laterally to the bregma, was performed, and the dura was surgically removed. The cortical tissue above the hippocampus was removed by aspiration (Kuga *et al.* 2011). Then, the exposed dorsal surface of the hippocampus was loaded with a small volume (approximately 4 μl) of dye solution consisting of 0.133% fluo-4 AM (Invitrogen), 100 μM SR101, 20% DMSO and 8% Pluronic F-127. During an incubation period of 60 min, the hippocampal surface was covered with a small piece of Gel Form (Pfizer Inc., New York, USA) to retain the dye solution in place. After the unloaded dye was washed with aCSF, the aspirated area was mounted with 2% agar dissolved in aCSF. The astrocyte calcium activity was imaged with a two-photon laser-scanning microscope based on a mode-locked Ti:sapphire laser with a 100 fs pulse width, 80 MHz pulse frequency and 840 nm wavelength (Mai Tai; Spectra Physics, Mountain View, CA, USA), an upright microscope (BX61WI; Olympus, Tokyo, Japan), and a water-immersion objective lens (20×, 0.95NA and 25×, 1.05NA, Olympus). After each experiment, the brain was removed and immediately frozen. Coronally sectioned preparations (30 μm thickness) were stained with 0.1% Cresyl Fast Violet (Wako Pure Chemical Industries, Osaka, Japan) to confirm the imaged area.

Electrophysiological recordings

Cell-attached patch-clamp recordings were obtained from neurons and astrocytes with an Axopatch 700B amplifier (Molecular Devices, Sunnyvale, CA, USA). Borosilicate glass pipettes (4–6 MΩ) were filled with aCSF. Signals were low-pass filtered at 1–2 kHz, digitized at 20 kHz and analysed with pClamp 10.1 software (Molecular Devices).

Calcium buffering

To inhibit astrocyte calcium activity, BAPTA was injected into the astrocytes. For a targeted single-cell electroporation technique, borosilicate glass pipettes (5–7 MΩ) were filled with aCSF containing 50 mM BAPTA (Sigma-Aldrich) and 1 mM Alexa Fluor 488 hydrazide (Invitrogen). The tip of the pipette was placed onto the soma in the same manner as for cell-attached recording, and 50 rectangular pulses (–5 V, 0.5 ms duration) were applied at a frequency of 50 Hz (Ohkura *et al.* 2012). This procedure was repeated in the adjacent astrocytes using the same pipette. For an alternative dialysis method, whole cell patch-clamp recordings were performed from astrocytes using borosilicate glass pipettes (5–7 MΩ) filled with a solution containing (in mM): 125 $KMeSO_4$, 10 Hepes, 4 $MgCl_2$, 4 ATP, 0.4 GTP, 10 BAPTA and 0.2 Alexa Fluor 594 (pH 7.2).

Calcium uncaging

To stimulate the astrocyte calcium signal, 10 mM *o*-nitrophenyl-EGTA (NP-EGTA; Invitrogen), a caged calcium reagent, was injected into the astrocytes using the electroporation described above. To lower the basal neuronal activity, the ionic composition of aCSF was modified as follows: 3.0 mM K^+, 1.8 mM Ca^{2+} and 1.8 mM Mg^{2+}. NP-EGTA was uncaged by a 150 μm diameter ultraviolet (UV) pulse for a 5–10 s exposure to UV light that was emitted from a 100 mW high-pressure mercury lamp (C-SHG1; Nikon, Tokyo, Japan) and short-pass filtered at 330 nm (XF1001; Omega Optical, Brattleboro, VT, USA).

Post hoc Nissl staining

Slices were fixed in 4% paraformaldehyde (PFA) in 0.1 M phosphate buffer solution for 2 h and were permeabilized with 0.3% Triton X-100 for 60 min. They were then incubated with 530/615 NeuroTrace Nissl (Invitrogen). Images were acquired at a *Z*-depth interval of 5 μm with an Olympus two-photon laser scanning system.

Immunohistochemistry

Rats (postnatal, 14 days old; $n = 5$) were perfused transcardially with cold 4% PFA in 25 mM phosphate-buffered saline (PBS). The brain samples were postfixed with 4% PFA overnight at 4°C. The fixed brains were rinsed three times with 25 mM PBS, and horizontal hippocampal slices with a thickness of 300 μm were prepared with a vibratome (Dosaka). Cultured slices were fixed in 4% PFA in 25 mM PBS overnight at 4°C. The slices were permeabilized in 25 mM PBS with 1% Triton X-100 and 10% goat serum at room temperature for 60 min. The samples were then incubated with primary rat monoclonal anti-NeuN antibody (1:1000; Millipore) and mouse monoclonal anti-S100β antibody (1:1000; Sigma) for two overnight periods at 4°C and labelled with secondary anti-rabbit IgG Alexa-488 (1:500; Life Technologies, Carlsbad, CA, USA) and anti-mouse IgG Alexa-594 (1:500; Invitrogen) overnight at room temperature.

Results

Slice preparations allow both imaging of cells with high spatiotemporal resolution and detailed manipulation of cell activity. A disadvantage of acute slices is that neuronal activity is almost abolished because most of the synaptic connections are severely disrupted. In cultured slices, synaptic connections can be re-established *ex vivo* (Wittner *et al.* 2007), and the spontaneous activity of neurons recovers to the some extent *in vivo* (Sasaki *et al.* 2007; Takahashi *et al.* 2010). To address how the astrocyte

calcium signal modulates intrinsic activity patterns in neuronal networks, we utilized cultured slice preparations. It has been suggested, however, that astrocytes change their fine structures and expression levels of proteins in slice preparations (Takano *et al.* 2014). We first confirmed how well the basic morphological and physiological properties of astrocytes were preserved in the cultured slices (Fig. 1). No significant differences were found in the density or the inter-soma distance of S100β-positive astrocyte pairs between *in vivo* preparations and cultured slices (Fig. 1*A*). The complexity of glial fibrillary acidic protein (GFAP)-positive processes was assessed by Sholl analysis. In the cultured slices, the number of intersections between the glial processes and the Sholl circles significantly decreased at distances of 20–40 μm and increased at distances greater than 60 μm from the glial soma (Fig. 1*B*, left; $P < 0.05$, Tukey's test). Branch order analysis revealed less cumulative branching in the cultured slices at any distance from the soma (Fig. 1*B*, right). These results suggest that cultured astrocytes have fewer branching structures, whereas individual processes are than those in *in vivo* astrocytes. GFAP-positive processes have been reported to be partially retracted shortly after the preparation of acute slices (Takano *et al.* 2014). Our results imply that after 1 week of incubation in culture, astrocytes are likely to re-extend the remaining processes without aberrant branching. Calcium imaging of the astrocytes showed that the basic kinetics of astrocyte calcium transients (i.e. duration and latency to peak) were not significantly different between the *in vivo* and cultured astrocytes (Fig. 1*D*; *in vivo*, $n = 533$ events from six animals; cultured slice, $n = 250$ events from seven slices), whereas the frequency of calcium activity tended to be lower in the cultured slices (Fig. 1*E*; *in vivo*, $n = 119$ active cells from six animals; cultured slice, $n = 98$ active cells from seven slices). Taken together, these results suggest

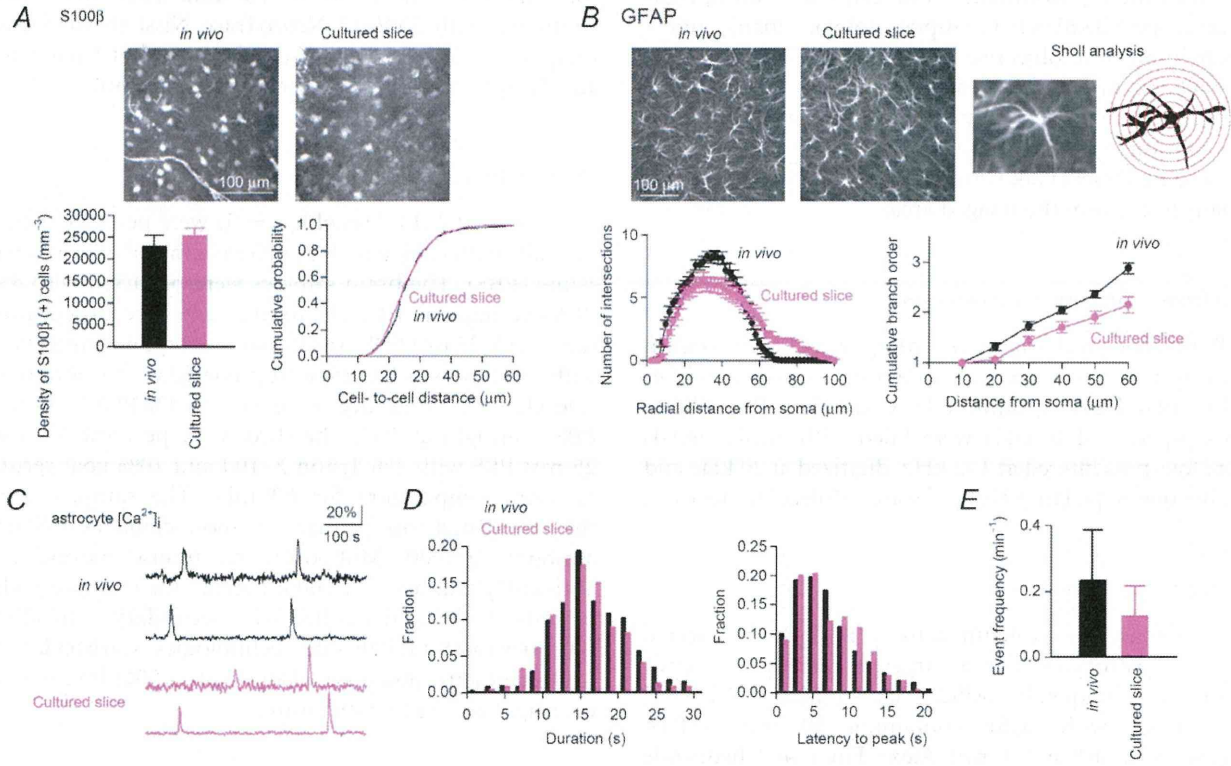

Figure 1. Morphological and physiological characteristics of astrocytes in cultured hippocampal slices
A, (*top*) immunolabeling of S100β in astrocytes in the striatum radiatum. The sections prepared by transcardial fixation are labelled *in vivo*. (*bottom*) Density of S100β-positive cells (left; $P > 0.05$, Student's *t* test, $n = 4$ slices each) and distribution of the cell-to-cell distances between the closest pairs of S100β-positive cells (right; $P > 0.05$, Kolmogorov–Smirnov test, *in vivo*, $n = 396$ cells; cultured slice, $n = 435$ cells). *B*, (*top*) immunolabelling of GFAP in astrocytes. An example cell used for Sholl analysis is magnified in the right panel. The red circles are depicted with diameters that increase in 10 μm intervals. (*bottom*) Sholl analysis of GFAP-positive processes (left; $n = 25$ cells each) and the cumulative branch order number plotted as a function of the path length from the soma (right). *C*, calcium fluorescence traces of rat astrocytes *in vivo* and in cultured slices. *D*, distribution of duration and latency to peak of the calcium events of astrocytes (*in vivo*, $n = 533$ events from six animals; cultured slice, $n = 250$ events from seven slices). *E*, average frequency of astrocyte calcium events (*in vivo*, $n = 119$ active cells from six animals; cultured slice, $n = 98$ active cells from seven slices). Error bars are SEM.

that the basic morphological and physiological properties are, at least in part, preserved in cultured astrocytes.

Imaging of neuronal and glial calcium activity in the hippocampus

Using a high-speed confocal imaging technique, we monitored the spatiotemporal patterns of the spontaneous activity of more than 100 neurons in the CA3 region of hippocampal slice cultures. Neurons and astrocytes were both loaded with OGB-1 AM and were discriminated based on *post hoc* staining with Nissl, a fluorescent neuron-specific marker (Fig. 2*A*). Compared with Nissl-negative cells, which correspond to putative glial cells, Nissl-positive neurons had larger somata (Fig. 2*C*) and a relatively lower basal fluorescence intensity (Sasaki *et al.* 2007). Cell-attached patch-clamp recordings revealed that the neurons exhibited calcium transients with a decay time constant of 350–600 ms in response to action potentials, whereas the astrocytes displayed slower calcium elevations with a duration of more than 2 s, independent of the electrical activity (Fig. 2*B* and *C*). Based on these morphological and functional characteristics, we were therefore able to separate neurons from astrocytes (Fig. 2*C*). We have previously reported that our imaging system can reliably detect the neuronal calcium events evoked by single spikes with 100% probability at a frame rate of 10 Hz (Sasaki *et al.* 2008). An example spatiotemporal activity pattern of neuronal and glial cells is shown in Fig. 2*D*. On average, the single movies included 100 ± 4 neurons and 29 ± 2 astrocytes ($n = 23$ slices). During our observation period of 5 min, $41 \pm 3\%$ neurons and $44 \pm 2\%$ astrocytes exhibited at least one calcium activity event. The frequencies of calcium activity were 3.6 ± 0.3 min^{-1} in active neurons ($n = 303$ cells) and 0.67 ± 0.04 min^{-1} in active astrocytes ($n = 68$ cells).

Evaluation of neuronal synchronization

We characterized the temporal correlation of the activity in a neuronal population. For any given short period of 100 ms, $0.36 \pm 0.05\%$ of the total recorded neurons ($n = 6$ slices) were active neurons. Thus, the spontaneous activity was fundamentally sparse. Nonetheless, the slices occasionally exhibited synchronized activity patterns (Fig. 2*D*). We frequently observed that a subset of neurons was recruited coincidently in these synchronized events. We thus defined a large synchronization as an event in which more than 10% of the total neurons exhibited calcium events during a period of 100 ms. To determine

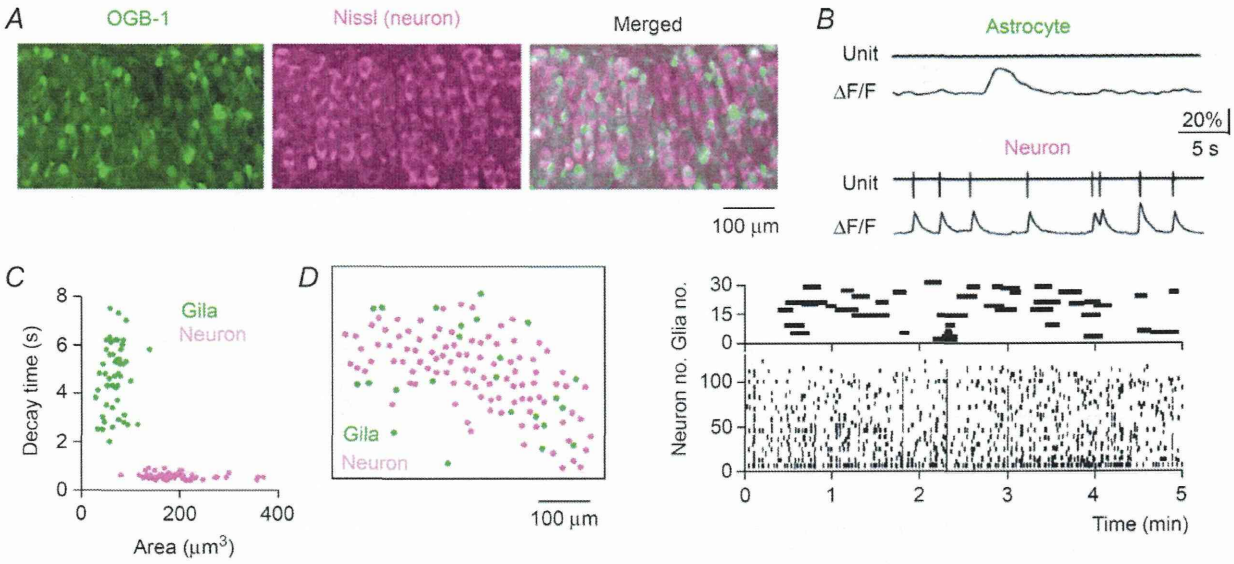

Figure 2. Optical recording of calcium activity in hippocampal neurons and glial cells
A, the hippocampal CA3 region in a cultured slice loaded with OGB-1 (*left*) was confocally imaged and *post hoc* Nissl-stained (*middle*). Non-neuronal cells became green in the merged image (*right*). *B*, an astrocyte (*top*) and a neuron (*bottom*) were patch-clamp recorded in the cell-attached configuration. The astrocytes exhibited spontaneous calcium elevations that were not associated with electrical activity, whereas the neurons exhibited calcium transients that were time-locked to action potentials. *C*, cell types were classified according to their size and the decay time constant of calcium activity. Putative astrocytes and neurons are indicated in green and magenta dots, respectively. Each dot indicates a single cell. *D*, the locations of 101 neurons and 24 astrocytes (left) in an imaged slice are shown in the left cell map. The spatiotemporal patterns of the spontaneous calcium events detected in these cells are plotted in the right rastergrams. Each black line represents a single calcium event. The recordings were performed in aCSF consisting of 4.5 mM K^+, 1.2 mM Ca^{2+} and 1.2 mM Mg^{2+}.

whether a stochastic process accounted for the large synchronization, we compared the emergence of large synchronization to that in randomized surrogate datasets. In the surrogate, we randomly shuffled the inter-event intervals (IEIs) of calcium events within each neuron and repeated this procedure for all neurons in the dataset (Fig. 3*A*). This procedure collapsed the temporal correlation across neuronal events without changing the total event number (Fig. 3*B*, right). For each dataset, we created 20 surrogates. An example surrogate is shown in Fig. 3*B*. The overall percentage of co-active neurons in the surrogates was shifted to the left in the cumulative probability distribution (Fig. 3*C* middle, $n = 6$ slices). Indeed, large synchronization emerged at a frequency of 1.7 ± 0.9 min^{-1} in the real datasets, but no large synchronization occurred in the surrogates (Fig. 3*C*). Therefore, the large synchronization in the original datasets could not be explained by chance.

To further confirm this notion, we utilized another prominent feature of neuronal activity, i.e. pairwise synchronization. The timings of calcium events are often correlated with a nearly zero time lag between two neurons. To quantify the level of synchrony, we calculated the correlation coefficients of event timings between pairs of neurons (Fig. 3*D*). The correlation coefficient had a mean of 0.10 ± 0.01 and ranged from 0.01 to 0.89 ($n = 8339$ pairs from 303 neurons in six slices). In surrogate datasets, this value decreased to 0.03 ± 0.01 and ranged from -0.04 to 0.19. We defined a highly correlated pair as a cell pair that exhibited a correlation coefficient greater than 0.25 because this level was not observed in the surrogate datasets. Indeed, the total number of correlated pairs was 36 ± 5 in the real datasets and 0 ± 0 in their surrogates (Fig. 3*D*). Therefore, in our preparations the neurons spontaneously generated temporally coordinated firing patterns. The average inter-soma distance between correlated neuron pairs was 81 ± 7 μm (Fig. 3*E*; $n = 246$ pairs).

Correlated activity between the neuronal and astrocytic population

We investigated whether astrocytes display calcium activity time-locked with neuronal synchronization (Fig. 4). The number of co-active glial cells correlated weakly but significantly with the percentage of co-active neurons (Fig. 4*B*; $n = 2741$; $R = 0.28$, $P < 0.01$). When more than 10% of the neurons showed synchronous activity, the glial cells increased the number of calcium events (Fig. 4*C*). This correlation analysis implies that glial cells are linked to the generation of neuronal co-activation. To examine the spatial relationship between neuronal and glial synchrony, we measured the inter-soma distances between co-active

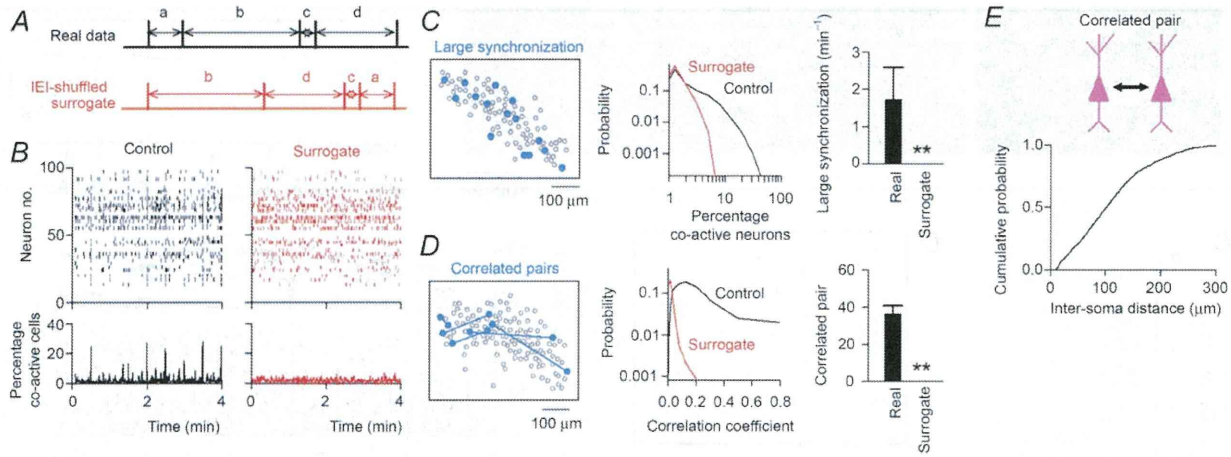

Figure 3. Characterization of synchronized neuronal activity in cultured hippocampal slices
A, to collate the event correlations between neurons, the inter-event intervals (IEIs) were transposed at random within cells. *B*, a rastergram of 100 neurons (*left*) was IEI shuffled (*right*). The *bottom* time histograms show the percentage of co-active neurons relative to the total number of imaged neurons (100 ms bin). *C*, cells activated during a representative large synchronization event are shown by filled circles in the *left* cell map. The distribution of the percentage of co-active cells during a time window of the 100 ms bin (*middle*) and the frequency of large synchronization (*right*) are compared with those in the corresponding surrogates ($n = 65{,}908$ bins from six slices). *D*, highly correlated neuron pairs, which exhibited correlation coefficients of more than 0.25, are linked by lines in the *left* cell map. The distribution of correlation values between all possible neuron pairs (*middle*) and the number of highly correlated neuron pairs (*right*) are compared with those in the corresponding surrogates ($n = 8339$ pairs from 303 neurons). Error bars are SEM, $^{**}P < 0.001$, paired *t* test. *E*, cumulative distribution of soma-to-soma distances between correlated neuron pairs ($n = 246$ pairs).